# Catalysis Science & Technology

Accepted Manuscript






ROYAL SOCIETY OF CHEMISTRY

www.rsc.org/catalysis

Journal Name

ARTICLE

# How $TiO_2$ facets determine arsenic adsorption and photooxidation: Spectroscopic and DFT study

Received 00th January 20xx,
Accepted 00th January 20xx

DOI: 10.1039/x0xx00000x

www.rsc.org/

Li Yan, Jingjing Du, Chuanyong Jing*

Anatase $TiO_2$ nanomaterials have been widely used in arsenic (As) remediation, although reports on their adsorption and photocatalytic capacity have been controversial. The motivation for our study is to explore the As adsorption and photooxidation processes on different $TiO_2$ facets at the molecular-level. Our results from multiple complementary characterization techniques suggest that anatase {001} facets have stronger Lewis acid sites than those on {101} facets, resulting in a higher As adsorption affinity. Density functional theory (DFT) calculations confirmed that the As surface complex is more energetically favorable on {001} than on {101} facets. In addition, the strong interaction of {001} facets with molecular $O_2$ facilitates the transfer of photo-excited electrons to the adsorbed $O_2$ to generate superoxide radical ($O_2^{\bullet-}$), which is the primary As(III) oxidant as evidenced by our radical-trapping experiments. Meanwhile, the oxygen vacancies on {001} facets could expedite the interfacial electron transfer and electron-hole separation, which promote the generation of $O_2^{\bullet-}$ and ultimately catalytic efficiency. The insights gained from this study provide a firm basis for the proposition that As adsorption and photoactivity can be mediated by tailoring the exposed $TiO_2$ facets, which is of essence in the design and application of $TiO_2$-based environmental technologies.

## 1. Introduction

Adsorption and photooxidation on $TiO_2$ nanomaterials provide a promising technique for arsenic (As) removal.[1] Though the As adsorption mechanism is well known to involve the formation of a bidentate binuclear surface complex,[2] even $TiO_2$ of the same anatase phase from different sources exhibit distinct adsorption and photo-catalytic capacities.[3-5] The lack of conformity of many experimental observations with the general belief that particle size or surface area regulates $TiO_2$ adsorption and photocatalysis motivates our study.

The adsorption and photocatalytic performance of anatase $TiO_2$ depend on its size, shape, and surface atomic structure.[6-8] Meanwhile, the properties of surface acid sites including type, concentration, and strength also play an important role in the activity of $TiO_2$.[9-12] In addition, the conduction band position[13] and the transport mobility of charge carriers including photo-excited holes ($h^+$) and electrons ($e^-$)[14] may influence photoreaction on anatase $TiO_2$. Mounting evidence over the past decade highlights the intrinsic complexity of the effects of structure on $TiO_2$ properties. However, the processes and associated molecular-level mechanisms that influence As adsorption and photooxidation on anatase $TiO_2$ remain enigmatic.

Recent intriguing studies have shown that the adsorption and photocatalytic activity of $TiO_2$ largely depend on its surface atomic structure and the degree of exposed reactive crystal facets.[15-17] The majority of exposed facets for most anatase are less-reactive and thermodynamically stable {101} facets (about 94%) with a minor proportion of {001} facets.[18] Conversely, water and dye molecules prefer to bind to anatase {001} rather than {101} facets.[17, 19-21] To the best of our knowledge, no publication has reported the $TiO_2$ facets effect on As adsorption. Nevertheless, the molecular level knowledge on $TiO_2$ facets determining As adsorption is of paramount importance in the design and implementation of $TiO_2$ in As remediation.

The high photocatalytic performance for anatase {001} facets has been explained by hydroxyl radical (•OH),[22] which is proposed to be the main oxidant for As(III) photooxidation in the $TiO_2$/UV system.[4, 23] In contrast, Choi et al. propose that instead of •OH, superoxide radical ($O_2^{\bullet-}$) should play a dominant role,[24, 25] which is supported by other independent studies.[26, 27] The controversy in the As(III) photooxidation mechanism may stem from the knowledge gap concerning the $TiO_2$ facets effect on the generation of reactive oxygen species (ROS). The generation of ROS such as •OH and $O_2^{\bullet-}$ is mediated by the reaction of surface-adsorbed $H_2O$ and $O_2$ molecules with photoexcited $h^+$ and $e^-$. Therefore, we hypothesize that anatase $TiO_2$ facets

*State Key Laboratory of Environmental Chemistry and Ecotoxicology, Research Center for Eco-Environmental Sciences, Chinese Academy of Sciences, Beijing 100085, China*
*Tel: +86 10 6284 9523; Fax: +86 10 6284 9523; E-mail: cyjing@rcees.ac.cn*
† Electronic Supplementary Information (ESI) available: [Structural characterization including XRD, BET, SEM, TEM, and XPS and detail of DFT calculations]. See DOI: 10.1039/x0xx00000x

may affect ROS generation and ultimately determine photocatalytic performance.

The objective of this study was to identify the primary factor influencing As adsorption and photocatalysis on anatase $TiO_2$, as well as its mechanism. Multiple complementary characterization methods and density functional theory (DFT) calculations were employed to explore the molecular-level processes on the {001} and {101} facets. The intrinsic facet-dependent mechanism obtained from this study would be fundamental in developing $TiO_2$-based environmental technologies with high adsorption capacity and photocatalytic activity.

## 2. Experimental

**Materials**

Three different kinds of $TiO_2$ nanoparticles (NPs), including one homemade (HM) and two commercial samples, were used in this study. The HM anatase $TiO_2$ was prepared by hydrolysis of titanyl sulfate as detailed in our previous study.[28] Commercial JR05 and TG01 anatase were obtained from Xuancheng Jingrui New Material Co., LTD (Anhui, China). Terephthalic acid (TA), ethylenediaminetetraacetic acid disodium salt (EDTA-2Na), 5,5-dimethyl-1-pyrroline-N-oxide (DMPO), and superoxide dismutase (SOD) from bovine liver were purchased from Sigma-Aldrich (St. Louis, US). *P*-benzoquinone was obtained from ACROS ORGANICS (Geel, Belgium). Dimethyl sulfoxide (DMSO) and isopropanol were purchased from Sinopharm Chemical Reagent Co., Ltd. (Shanghai, China). Stock solutions of arsenic were prepared using $Na_2HasO_4 \cdot 7H_2O$ and $NaAsO_2$ (Fisher Sci., US). Milli-Q water was used to prepare solutions.

**As(III) and As(V) adsorption**

Adsorption isotherm experiments were performed to determine the As(III) and As(V) adsorption capacity on the three types of $TiO_2$ in 0.04 M NaCl solution. Suspension samples containing 0.31-3450 mg/L As(III) or 0.32-4484 mg/L As(V) and 5 g/L $TiO_2$ were adjusted to pH 7 with NaOH and HCl. The samples were covered with aluminum foil to prevent light exposure and mixed on a rotator for 72 h. Then, the final pH was measured and the suspensions were filtered through a 0.22-μm membrane filter for measurement of soluble As using a furnace atomic absorption spectrometer (FAAS, Perkin-Elmer AAS-800) with a detection limit of 0.7 μg/L.[29]

**As(III) photooxidation**

As(III) photooxidation experiments were carried out in an Erlenmeyer flask with 14 mg-As(III)/L in a suspension containing 0.3 g/L $TiO_2$ and 0.04 M NaCl at pH 7. The sample was stirred in the dark for 2 h to achieve equilibrium before being illuminated by a tubular mercury UV lamp (CEL-WLPM10-254, wavelength 254 nm) with an incident light intensity of about 4000 μW/cm$^2$. A control experiment in the dark was also performed. The photocatalysis process was monitored as a function of illumination time by taking 1 mL aliquots from the suspension and filtering through a 0.22-μm membrane. The As concentration and speciation were determined using high performance liquid chromatography (HPLC) coupled with a hydride generation atomic fluorescence spectrometer (HG-AFS, Jitian, P.R. China) with a detection limit of 0.7 μg/L for As(III) and 1.7 μg/L for As(V).[30]

**ROS species measurement**

The •OH radical measurement followed the procedure described in a previous report.[31] Terephthalic acid (TA) was used as a fluorescence probe because it can react with •OH to generate 2-hydroxy terephthalic acid (TAOH), which emits a unique fluorescence band at around 426 nm. $TiO_2$ samples (62.5 mg) were suspended in 250 mL solution containing 3 mM TA, and the suspension was stirred in the dark for 2 h to reach equilibrium. Then, the sample was illuminated with UV light, and 2 mL aliquots were taken out every 15 min and immediately filtered through a 0.22-μm membrane for fluorescence measurement. The photoluminescence (PL) emission spectra were recorded with a spectrofluorometer (Hitachi F-4500, Japan) with an excitation wavelength at 312 nm.

The electron spin resonance (ESR) signal of the radicals spin-trapped by DMPO was recorded on a BRUKER EMX plus spectrometer after 30 s photoirradiation with an 100 W mercury lamp (LOT-Oriel Gmbh&Co. KG). The settings were as follows: center field at 3503 G, microwave frequency at 9054.6 MHz, and power at 0.998 mW.

**Zeta (ζ) potential measurement**

To study the pHzpc of $TiO_2$ NPs, ζ potential was measured using a Zetasizer Nano ZS (Malvern Instrument Ltd., UK). The pH of the suspension containing 0.2 g/L $TiO_2$ in 0.04 M NaCl was adjusted between 3 and 9 using NaOH and HCl. Suspension samples were placed on a rotating shaker for 24 h and the final pH was measured. The reported ζ potential value was the average of three measurements.

**Characterization**

The crystal structures of the three $TiO_2$ samples were determined by powder X-ray diffraction (XRD) using an X'Pert PRO diffractometer (PANalytical, Netherlands) with Cu Kα radiation. The shape and morphology were characterized by a field-emission scanning electron microscope (FE-SEM, SU-8020, Hitachi) and transmission electron microscope (TEM, JEM-2100 from JEOL. Ltd). The Brunauer-Emmet-Teller (BET) specific surface area and Barrett-Joyner-Halenda (BJH) pore size distribution were determined from $N_2$ adsorption-desorption isotherms measured at 77 K using an automated gas sorption instrument (Quantachrome Instruments U.S. Autosorb-iQ) after the samples were degassed at 105 $^o$C for 12 h. The amount of acid sites was estimated from $NH_3$ temperature programmed desorption ($NH_3$-TPD) measurements performed by a Quantachrome TPRWinV3.51 system (Quantachrome Instruments U.S. ChemBET Pulsar TPR/TPD). The acid properties were also examined by FTIR spectra of pyridine adsorption samples using a Thermo-Nicolet Nexus 6700 FTIR spectrometer. Raman

measurements were performed on a Horiba JY HR800 Raman spectrometer with an exciting wavelength at 633 nm. UV-vis diffuse reflectance spectra (DRS) were obtained using a scan UV-vis spectrophotometer (DRS, UV-2450) equipped with an integrating sphere assembly, while $BaSO_4$ was used as a reference. X-ray photoelectron spectroscopy (XPS) and X-ray photoelectron valence-band (VB) spectra were measured on a Thermo SCIENTIFIC ESCALAB 250 spectrometer with Al Kα X-ray radiation at 1486.8 eV.

**Computational details**

DFT calculations were conducted to investigate the effect of $TiO_2$ facets on the As adsorption and photocatalysis. The plane-wave based calculations were performed using the Castep package in Materials Studio (Accelrys, San Diego, CA).[32] The model-building procedures were similar to our previous study and detailed in the electronic supplementary information (ESI†).[33] A plane-wave cutoff energy of 340 eV was selected during the calculations. Ultrasoft pseudopotentials available with the package were used in the treatment of core electrons. Exchange-correlation energy was calculated with the generalized gradient approximation (GGA) approach of Perdew-Burke-Ernzerhof (PBE).[34] The *k*-point over the Brillouin zone was set as a 1×2×1 grid due to the large size of the slab model. The BFGS method was employed for geometry optimization until the SCF and energy tolerances were less than the convergence criteria, $1.0 \times 10^{-6}$ and $1.0 \times 10^{-5}$ eV/atom, respectively.[33]

## 3. Results and discussion

**Characterization**

The three types of $TiO_2$ NPs were in the anatase phase (Table 1 and Fig. S1). The XRD-derived particle size was in reasonable agreement with that obtained from the BET surface area, $S_{BET}$ (Fig. S2), and the TEM analysis (Fig. S3). All $TiO_2$ samples had comparable surface components in the same chemical states as evidenced by XPS (Fig. S4). Detailed structural characterization and comparison of the three $TiO_2$ NPs are shown in Table S1.

**Table 1** Summary of characterization of three $TiO_2$ NPs.

| Sample | HM | JR05 | TG01 |
|---|---|---|---|
| Crystalline phase | anatase | anatase | anatase |
| XRD crystal size (nm) | 4.6 | 7.5 | 18.4 |
| $S_{BET}$ ($m^2$/g) | 336 | 167 | 71 |
| Acid concentration (mmol/g) | 0.078 | 0.036 | 0.043 |
| Exposed {001} facet (%) | 4 | 17 | 7 |
| pHzpc | 5.3 | 6.5 | 6.1 |
| As(III) adsorption capacity (mg/g) | 136 | 138 | 71 |
| As(V) adsorption capacity (mg/g) | 140 | 144 | 106 |
| As(III) surface coverage (molecules/$nm^2$) | 3.2 | 6.6 | 8.0 |
| As(V) surface coverage (molecules/$nm^2$) | 3.3 | 6.9 | 12.0 |
| As(III) loading (mol/mol acid) | 23.2 | 51.1 | 22.0 |
| As(V) loading (mol/mol acid) | 23.9 | 53.3 | 32.9 |
| As(III) photooxidation rate $k$×10000 ($min^{-1}$) | 60.0 | 213 | 225 |

**$S_{BET}$ effect on adsorption capacity**

The adsorption isotherms of As(III) and As(V) on the three $TiO_2$ NPs conformed to the Langmuir model (Fig. 1a-b), and the fitting parameters are shown in Table S2. Unexpectedly, no linear dependence was observed for the maximum adsorption capacity ($q_m$) on $S_{BET}$ or particle size (Fig. 1c-d). For example, the $S_{BET}$ of JR05 (167 $m^2$/g) was about half that of HM (336 $m^2$/g); however, the $q_m$ of JR05 for As(III) (138 mg/g) and As(V) (144 mg/g) were comparable to those of HM (136 and 140 mg/g, respectively, for As(III) and As(V)) (Table 1). Similarly, the adsorption density in the unit of molecules/$nm^2$ was not proportional to the particle size (Fig. 1d). Specifically, HM, with the smallest particle size (4.6 nm), resulted in the lowest As adsorption density (<3.5 molecules/$nm^2$). In contrast to the general belief that $q_m$ depends on $S_{BET}$ or particle size,[8] our results suggest that $S_{BET}$ or particle size may not be the key factor influencing the As adsorption capacity on $TiO_2$ NPs.

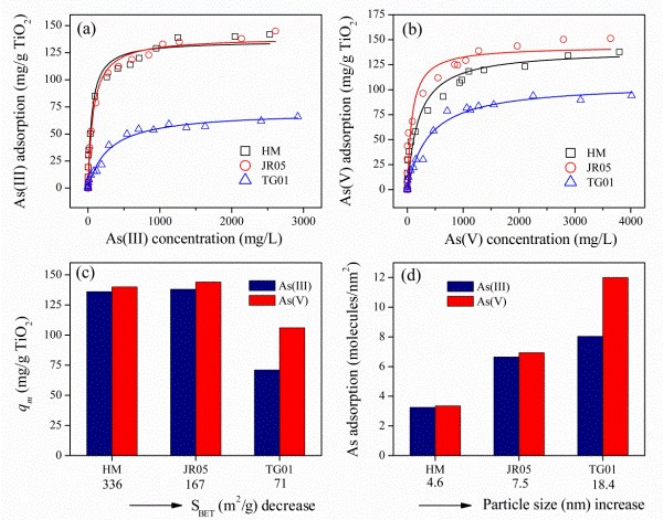


**Fig. 1** Adsorption isotherms of As(III) (a) and As(V) (b), the maximum adsorption capacity (c) and adsorption density (d) on three $TiO_2$ NPs.

**Effect of surface acid sites**

The type and concentration of acid sites were determined by pyridine-adsorbed FTIR spectra and $NH_3$-TPD analysis, respectively. Only the Lewis type of acid sites existed on the surfaces of the three $TiO_2$ NPs (Fig. 2a), and the acid site concentration was not proportional to the adsorption capacity (Table 1). For instance, JR05 exhibited the highest As(V) adsorption capacity (144 mg/g), while having the lowest acid concentration (0.036 mmol/g) among all three $TiO_2$ NPs. This observation indicates that the concentration of total acid sites may not be the determining parameter in As adsorption on $TiO_2$.

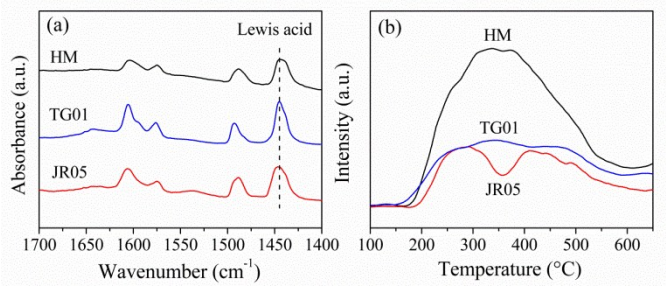


**Fig. 2** Pyridine-adsorbed FTIR spectra (a) and $NH_3$-TPD profiles (b) of three $TiO_2$ NPs.

Notably, the acid-site-normalized loadings of As(III) and As(V) on JR05, 51.1 and 53.3 mol/mol acid, respectively, were approximately twice as high as for the other two $TiO_2$ NPs (Table 1). This observation suggests that the acid sites on JR05 have a greater strength. This premise was further confirmed by our $NH_3$-TPD result, where a distinctive peak in the $NH_3$ desorption curve of JR05 was observed at about 410 ℃, corresponding to about 46% strong acid sites (Fig. 2b).[35] In contrast, the other two NPs exhibited a homogenous distribution of weaker acid sites on the surface.

The distribution of acid sites is closely related to surface atomic coordination and arrangement, indicating that different crystal facets may endow the same Lewis acid sites with different strengths. This assumption was justified by our DFT calculations for the adsorption of $NH_3$, a probe molecule, on $TiO_2$ {001} and {101} facets (Fig. S5). The $NH_3$ adsorption energies were estimated to be -2.43 and -1.14 eV for {001} and {101} facets, respectively (Fig. 3), indicating that {001} facets exhibit stronger acid sites than those on {101} facets.[9] We then proposed that the high As adsorption capacity on JR05 should be related to its exposed facets and their relative proportions, and this hypothesis was justified by the following quantum chemistry calculations.

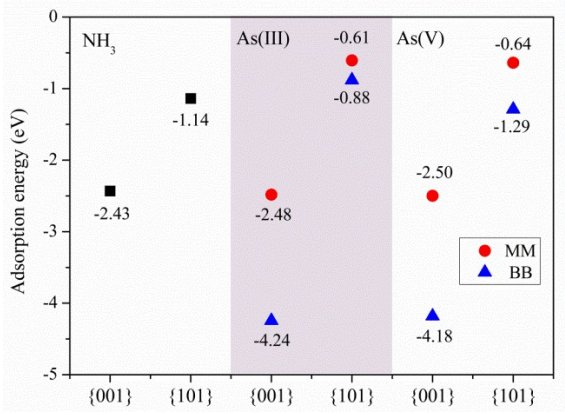


**Fig. 3** DFT calculated $NH_3$ (left), As(III) (middle), and As(V) (right) adsorption energies on anatase {001} and {101} facets with bidentate binuclear (blue triangles) and monodentate mononuclear (red circles) surface configurations. The structure parameters for optimized adsorption complexes and the calculation of adsorption energies are detailed in the ESI†.

**Facet dependence of As adsorption energy**

To explore the facets effect, DFT calculations were performed to compare the As adsorption energies for bidentate binuclear (BB) and monodentate mononuclear (MM) inner-sphere complexes on $TiO_2$ {001} and {101} facets (Fig. S6-S7). The results are summarized in Fig. 3 and highlight two observations. First, BB complexes are more stable than MM on both facets as evidenced by their more negative adsorption energies (Table S4), in agreement with previous reports.[36, 37] Second, both BB and MM complexes are more energetically favorable on {001} than on {101} facets. In fact, the adsorption energy for the BB configuration on {001} facets was 3.36 and 2.89 eV more negative than on {101} facets for As(III) and As(V), respectively. The As adsorption mechanism on $TiO_2$ was further elucidated using partial density of state (PDOS). The overlap of PDOS in Fig. S8-S9 indicated that the five-coordinated $Ti_{5c}$ atoms on the facets could form chemical bonds with O atoms from As oxoanions, where the newly formed Ti-O bonds were mainly attributed to the electron sharing between the O-2*p* and Ti-3*d* orbitals.[33]

$TiO_2$ {001} and {101} facets, having different surface atomic structures, exhibited distinct abilities in anchoring As. Notably, $TiO_2$ {001} facets provide 100% five coordinated ($Ti_{5c}$) sites as compared to 50% $Ti_{5c}$ on the {101} facets.[17, 38] The different density of these highly reactive unsaturated $Ti_{5c}$ sites contributes to the variation in adsorption capacity for the facets. Thus, the higher proportion of exposed {001} facets with strong Lewis acid sites on JR05 gave rise to its high As adsorption capacity. This conclusion was justified by our Raman analysis (Fig. 4a, Table S3), which implied that JR05 exposed 17% {001} facets, much more than the other two $TiO_2$ samples (4-7%). The % values refer to the facet area and not the number of facets. The As adsorption behaviors on $TiO_2$ NPs can also be evidenced by their pHzpc (Fig. 4b, Table 1), which showed that JR05, with a high proportion of {001} facets, exhibited the highest pHzpc (6.5), leading to a high adsorption affinity, consistent with our DFT calculations (Fig. 3). Though As adsorption removal using $TiO_2$ is well studied and applied, research investigating the $TiO_2$ facets effect on As adsorption has been rare. However, our molecular-level insights on how {001} facets determine As adsorption should be of paramount importance in the design and implementation of $TiO_2$ in As remediation as well as in other environmental applications.

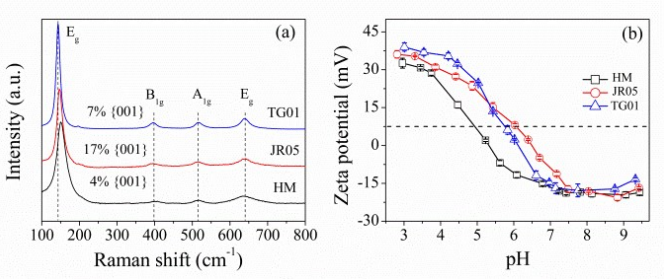


**Fig. 4** Raman spectra of three $TiO_2$ NPs (a) and Zeta potential of 0.2 g/L $TiO_2$ as a function of pH (b).

### As(III) photooxidation on three types of $TiO_2$

In addition to its high adsorption capacity, $TiO_2$ also exhibits effective As(III) photocatalytic oxidation.[4, 24, 39] The plot of As(III) to initial As(III) ($C/C_0$) versus irradiation time shown in Fig. 5 suggests that As(III) oxidation on the surfaces of the three $TiO_2$ NPs follows first-order kinetics.[8, 39] The first-order rate constant, $k$, varied in the order TG01 (0.0225 $min^{-1}$) > JR05 (0.0213 $min^{-1}$) > HM (0.006 $min^{-1}$) (Table 1). No oxidation of As(III) to As(V) was observed in the absence of $TiO_2$ (Fig. S10) and the control experiment indicated that As(III) oxidation is negligible under dark conditions. The different As(III) photooxidation rate on the three $TiO_2$ NPs inspired our further study to characterize on ROS effects.

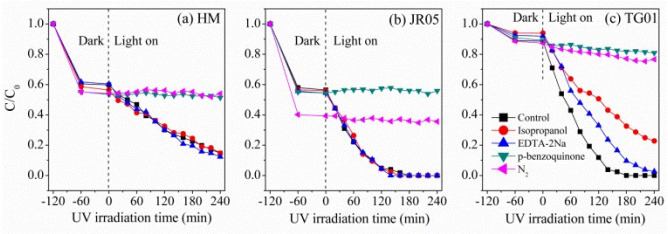


**Fig. 5** As(III) oxidation kinetics with addition of different scavengers (isopropanol: •OH scavenger; EDTA-2Na: $h^+$ scavenger; p-benzoquinone: $O_2^{\bullet-}$ scavenger) for HM (a), JR05 (b), and TG01 (c). Initial As(III) = 14 mg/L; $TiO_2$ = 0.3 g/L; pH = 7.

### Identify ROS in As(III)-$TiO_2$/UV system

Reactive oxygen species (ROS), including •OH and $O_2^{\bullet-}$, are commonly accepted as the main oxidants in the $TiO_2$/UV process.[4, 24, 40, 41] Our ESR and fluorescence experimental results show that both •OH and $O_2^{\bullet-}$ existed for all $TiO_2$ samples (Fig. 6, Fig. 7). The amount of •OH followed the order TG01 > JR05 > HM (Fig. 7, Fig. S11). By comparing the ESR signal after addition of 10% DMSO (•OH scavenger) and 0.05 g/L SOD ($O_2^{\bullet-}$ scavenger) to 0.1 g/L $TiO_2$ dispersions, the amount of $O_2^{\bullet-}$ present during photooxidation was found to follow the order JR05 > TG01 > HM (Fig. 6).

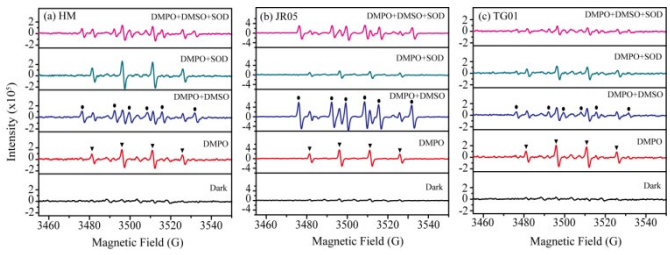


**Fig. 6** Electron spin resonance spectra of radical adducts trapped by DMPO in HM (a), JR05 (b), and TG01 (c) dispersions after 30 s UV irradiation with addition of different scavengers (DMSO: •OH scavenger; SOD: $O_2^{\bullet-}$ scavenger). DMPO–·OH radical and methyl radical are labeled by triangles and circles, respectively.

To compare the contributions of •OH, $O_2^{\bullet-}$, and photogenerated holes ($h^+$) to As(III) photooxidation, the photocatalytic reaction was investigated using the radical trapping technique with three selective radical scavengers and $N_2$ purging. The results in Fig. 5 show that the As(III) oxidation in TG01 was appreciably suppressed by 74% and 34%, respectively, after addition of isopropanol (•OH scavenger, 200 mM)[42, 43] and EDTA-2Na ($h^+$ scavenger, 40 mM).[44] In contrast, no discernable difference was observed in the As(III) oxidation upon the removal of •OH and $h^+$ in HM and JR05. Notably, 40 mM *p*-benzoquinone, an $O_2^{\bullet-}$ scavenger,[45] almost inhibited all As(III) photooxidation for the three types of $TiO_2$ NPs (Fig. 5, Table 2). This result strongly indicates that $O_2^{\bullet-}$ dominated As(III) photooxidation on $TiO_2$,[24, 27, 41] and •OH and $h^+$ were involved for TG01, but not for HM and JR05.

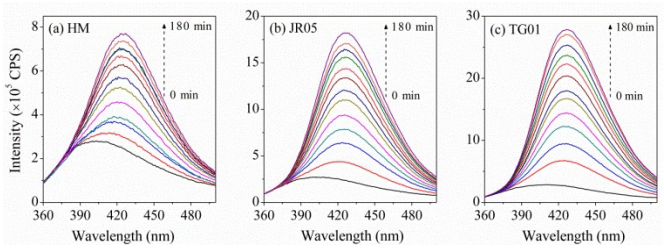


**Fig. 7** Fluorescence spectra of the UV irradiated $TiO_2$ suspensions in 3 mM terephthalic acid at different irradiation time: (a) HM, (b) JR05, and (c) TG01.

**Table 2** As(III) photooxidation rate constants on three $TiO_2$ NPs with addition of different scavengers.

| | First-order Constant: k×10000 ($min^{-1}$) | | | | |
|---|---|---|---|---|---|
| $TiO_2$ Samples | Control | •OH scavenger (isopropanol) | $h^+$ scavenger (EDTA-2Na) | $O_2^{\bullet-}$ scavenger (*p*-benzoquinone) | $N_2$ |
| HM | 60.0 | 53.0 | 67.2 | 0 | 0 |
| JR05 | 213 | 228 | 200 | 0 | 0 |
| TG01 | 225 | 58.0 | 149 | 3.39 | 5.61 |

### Facet effect on $O_2^{\bullet-}$ formation

$O_2^{\bullet-}$ formation is the result of the trapping photogenerated electrons by molecular $O_2$ adsorbed on the $TiO_2$ surface under UV irradiation.[14] Our results in Fig. 5 show that the removal of dissolved $O_2$ by purging with $N_2$ led to the same level of suppression on As(III) photooxidation for the three $TiO_2$ NPs as *p*-benzoquinone, which confirmed that adsorbed $O_2$ could act as a photogenerated electron scavenger to produce $O_2^{\bullet-}$ and subsequently oxidize As(III). Because different $TiO_2$ facets exhibit distinct adsorption affinities for $NH_3$ and As (Fig. 3), a reasonable postulation is that the exposed $TiO_2$ facets would influence the adsorption of molecular $O_2$, and as a result, affect the formation of $O_2^{\bullet-}$.

To understand the facet effect on $O_2^{\bullet-}$ generation, DFT calculations were performed with molecular $O_2$ associated with a $Ti_{5c}$ atom on {001} and {101} facets. The optimized structure in Fig. 8 shows a significant structural disorder on the {001} facets, resulting in a more negative adsorption energy

(-2.48 eV) and shorter Ti-O bond distance (2.012 Å) compared to those on {101} facets (-1.79 eV and 2.033 Å, respectively).

The strong interactions between $O_2$ and $TiO_2$ {001} facet may facilitate the electron transfer from the surface to $O_2$, forming $O_2^{\bullet-}$. Analysis of Mulliken charge shows that {001} facets could donate a 0.39 charge to an adsorbed $O_2$ molecule. This charge transfer process would expedite the consumption of photoelectrons and thus prevent their immediate electron-hole recombination, which is beneficial to the photocatalytic activity.[6]

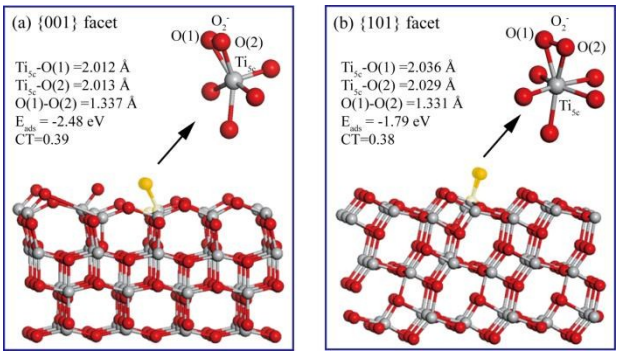


**Fig. 8** Optimized geometries of $O_2^-$ molecule adsorbed at the $Ti_{5c}$ site on anatase {001} facets (a) and {101} facets (b). CT: charge transfer from $TiO_2$ facets to the adsorbed $O_2$ molecule, which is calculated by subtracting Mulliken charge of isolated $O_2$ from that of $O_2$ after adsorption on $TiO_2$ facets. Note: Superoxide $O_2^-$ anion is added from the beginning by adding an extra electron to the system. The optimized geometric parameters and the calculation of adsorption energies are detailed in the ESI†.

It should be noticed that according to previous study,[46] the photogenerated electrons are mainly located in the subsurface atomic layer of {001} facets. Thus, an energy barrier should prevent the transfer of electrons from subsurface $Ti_{6c}$ sites to surface $Ti_{5c}$ sites. We hypothesize that the surface distortion after $O_2$ adsorption could promote the transfer of electrons from the subsurface atomic layer (the initial electron trapping sites) to the outermost atomic layer (where photocatalytic reactions generally occur). Therefore, we compared the surface distortion of {001} and {101} facets after adsorption.

As shown in Fig. 8, a substantial surface distortion was obtained for $O_2$ adsorption on {001} facets compared with that on {101} facets. The energy obtained from surface distortion on {001} facets was 0.92 eV (Table S5), which was capable to overcome the electron trapping energy barrier on {001} facets (0.38 eV).[46] Such an energy difference could facilitate the electron transfer from subsurface $Ti_{6c}$ sites to surface $Ti_{5c}$ sites.[47] This results suggest that the strong affinity of $O_2$ on {001} facets and the significant surface distortion can synergistically enhance the separation of photogenerated electrons and holes.

The surface distortion induced by As(III) adsorption may also facilitate the electron transfer and lead to the change in local potential. The energy obtained from surface distortion upon As(III) adsorption on {001} facets was 1.27 eV and 3.42 eV for MM and BB surface complexes (Table S5), respectively, which is sufficiently high to overcome the energy barrier for the electron transfer from bulk to surface. Further understanding the change in local potential for the outermost and inner atomic layers with surface distortion was obtained by examining the projected densities of states (PDOS) on Ti atoms in different atomic layers on {001} and {101} facets.

As shown in Fig. S12a-b, the PDOS for Ti atoms in the first (Ti1), second (Ti2), and third (Ti3) layers on {001} facets almost overlap (top half in each panel), indicating that almost no energy gradient exists to drive the flow of photogenerated electrons from the bulk to the surface layer. On the other hand, upon As(III) adsorption and surface distortion, the energy levels of the three Ti atoms were appreciably decreased by approximately 1.7 eV. The states of Ti1 and Ti2 became the lowest-lying one (-7.1 eV) for both MM and BB surface complexes (bottom half), whereas Ti3 resulted in a higher state at -6.7 eV. The energy difference between surface and bulk Ti atoms (0.4 eV) enables the flow of electrons from the bulk region to the surface layer.[47] However, such a change in local potential was negligible on {101} facets (Fig. S12c-d), indicating the insignificant effect of As(III) adsorption on {101} surface distortion and electron transfer.

**Surface electronic structure effect on photoactivity**

The electronic band structure was analyzed to examine the effect of the transport mobility of charge carriers on photoactivity, and the results are shown in Fig. 9. The UV-vis absorption spectra (Fig. 9a) demonstrated that HM and JR05 resulted in comparable absorbance with nearly overlapping absorption edges, whereas the absorption edge of TG01 exhibited a red-shift of about 6 nm with respect to those of HM and JR05. Thus, the band gaps followed the order HM ≈ JR05 > TG01. The X-ray photoelectron valence-band (VB) spectra (Fig. 9b) revealed that the VB maxima of the three $TiO_2$ samples were at about 2.87 eV, in line with a previous report (2.93 eV). [40]

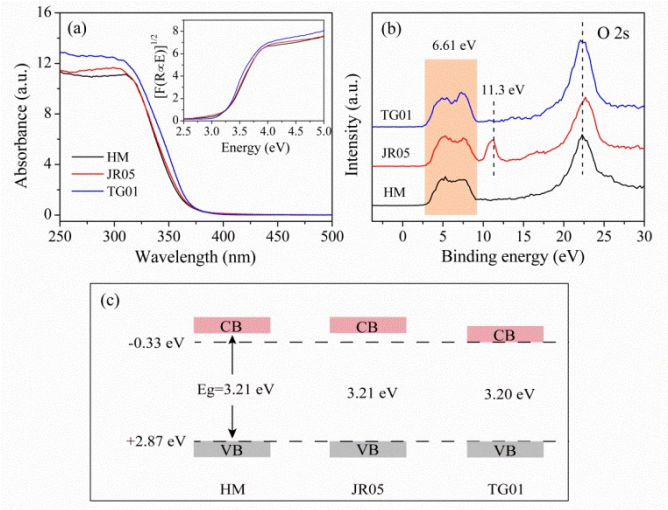


**Fig. 9** (a) UV-vis absorption spectra of HM, JR05, and TG01 and the inset showing their transformed Kubelka-Munk functions as a function of energy. (b) X-ray

photoelectron valence-band (VB) spectra of three $TiO_2$. (c) Valence-band and conduction-band edges of HM, JR05, and TG01 determined from spectra.

The resolved band structures of three $TiO_2$ are illustrated in Fig. 9c. The nearly identical widths of valence bands for HM and TG01 (about 6.61 eV) indicated that the charge carriers (photo-excited electrons and holes) of these two $TiO_2$ had similar mobility.[13] On the other hand, JR05 exhibited a wider valence band with an additional peak at about 11.3 eV (Fig. 9b), indicating the existence of oxygen vacancies as the result of exposed {001} facets.[13, 48, 49] Because high-energy {001} facets are characterized by unsaturated five-coordinated $Ti_{5c}$ atoms and large Ti-O-Ti bond angles (144.9 ° compared to 101.9 ° for {101} facets), substantial oxygen deficiency may occur.[16, 50, 51] Such an oxygen vacancy can increase the transport mobility of charge carriers and thus reduce the possibility of recombination of electron-hole pairs.[52]

Our molecular-level insights indicate that As(III) photooxidation on $TiO_2$ can be simultaneously tuned through the synergistic effects of surface atomic structure and surface electronic structure. The {001} facets with 100% $Ti_{5c}$ atoms exhibited stronger interactions with molecular $O_2$ as evidenced by the shorter Ti-O bond distance (2.012 Å) than that on {101} facets (2.033 Å). Its unique surface atomic structure resulted in a more negative adsorption energy (-2.48 eV) compared with that on {101} facets (-1.79 eV) (Fig. 8), which could facilitate the charge transfer (CT=0.39) from {001} facets to adsorbed $O_2$ to generate $O_2^{\bullet-}$. In addition, the electronic structure of {001} facets with abundant oxygen vacancies facilitated the mobility of the charge carriers (Fig. 9b), which should expedite the interfacial electron transfer and electron-hole separation, and subsequently promote $O_2^{\bullet-}$ generation and As(III) oxidation. This synergistic effect could explain the higher photoreactivity of JR05 (0.0213 $min^{-1}$) with 17% {001} facets compared with HM (0.006 $min^{-1}$) with only 4% {001} facets.

Notably, our conclusion on the preference of $O_2^{\bullet-}$ generation on {001} facets is in apparent contradiction with previous studies which propose that $O_2^{\bullet-}$ generation on {101} facets is favorable due to their reductive properties.[53, 54] Though reductive {101} facets with more photoelectrons are favorable for the formation of $O_2^{\bullet-}$, we believe the adsorption of molecular $O_2$ should be the main factor in $O_2^{\bullet-}$ generation. The $O_2$ adsorption on {001} facets had a higher affinity than on {101} facets (Fig. 8). Furthermore, the photoelectrons anchored on subsurface atomic layers on {001} facets can be transferred to the outermost atomic layer to reduce $O_2$ and generate $O_2^{\bullet-}$ (Fig. 8 and Table S5). Meanwhile, the synergistic effect of facet-derived oxygen deficiency on photocatalytic performance should be considered in addressing $O_2^{\bullet-}$ generation on different facets.

JR05 and HM were the two $TiO_2$ NPs involving only $O_2^{\bullet-}$ in the photocatalysis, and the generation of more $O_2^{\bullet-}$ on JR05 can be evidenced indirectly by the amount of As(III) adsorption under a $N_2$ environment. In fact, the As(III) adsorption density was increased 21.6% under a $N_2$ environment compared to that of control sample (Fig. 5). This pronounced increase could be ascribed to the greater number of available $Ti_{5c}$ sites to adsorb As(III) under the $N_2$ condition because $N_2$ is inert toward the $TiO_2$ surface. On the contrary, $O_2$ molecules can occupy the $Ti_{5c}$ sites to generate $O_2^{\bullet-}$, which reduces the As(III) adsorption density on the surface.

It should be noticed that though JR05 exposed a higher proportion of {001} facets (17%) than TG01 (7%) and generated more $O_2^{\bullet-}$ as evidenced by ESR results (Fig. 6), the photocatalytic rate of JR05 (0.0213 $min^{-1}$) was slightly lower than that of TG01 (0.0225 $min^{-1}$). The high photoactivity of TG01 could be attributed to the contribution of •OH and $h^+$ as evidenced by our radical trapping experiments, and the reason for different ROS involved in $TiO_2$ photocatalysis is worth further study.

## 4. Conclusions

This work exploited structural effects on the adsorption and photocatalytic performance of $TiO_2$. Contrary to the traditional concept that particle size or specific surface area is the main factor influencing As adsorption on $TiO_2$ NPs, we found that the distribution of exposed crystal facets is the key factor. $TiO_2$ {001} facets, with stronger Lewis acid $Ti^{4+}$ atoms, exhibit higher adsorption affinity than {101} facets. Furthermore, the strong interactions of {001} facets with oxygen molecules lead to more photoelectrons being transferred to the adsorbed $O_2$ to generate superoxide radical, which is the primary oxidant in the As(III) photooxidation. Our experimental and theoretical results provide new insights into the intrinsic origin of the facet-activity relationship. The results obtained from this study highlight the importance of crystal facets in adsorption and photocatalysis, which is of essence in the design and application of $TiO_2$ NPs with high adsorption ability and photocatalytic activity. In addition, the mechanism of the facet dependence of adsorption and photocatalysis should be applicable to other pollutant molecules beyond arsenic.

## Acknowledgements

We acknowledge the financial support of the National Basic Research Program of China (2015CB932003), the Strategic Priority Research Program of the Chinese Academy of Sciences (XDB14020201), the National Natural Science Foundation of China (41373123, 41425016, 21337004).

## Notes and references

1 X. Guan, J. Du, X. Meng, Y. Sun, B. Sun and Q. Hu, *J. Hazard. Mater.*, 2012, **215**, 1-16.
2 M. Pena, X. Meng, G. P. Korfiatis and C. Jing, *Environ. Sci. Technol.*, 2006, **40**, 1257-1262.
3 P. K. Dutta, A. K. Ray, V. K. Sharma and F. J. Millero, *J. Colloid Interface Sci.*, 2004, **278**, 270-275.
4 P. K. Dutta, S. O. Pehkonen, V. K. Sharma and A. K. Ray, *Environ. Sci. Technol.*, 2005, **39**, 1827-1834.
5 G. Jegadeesan, S. R. Al-Abed, V. Sundaram, H. Choi, K. G. Scheckel and D. D. Dionysiou, *Water Res.*, 2010, **44**, 965-973.
6 Y.F. Li and Z.P. Liu, *J. Am. Chem. Soc.*, 2011, **133**, 15743-15752.
7 X. Chen and S. S. Mao, *Chem. Rev.*, 2007, **107**, 2891-2959.
8 Z. Xu and X. Meng, *J. Hazard. Mater.*, 2009, **168**, 747-752.
9 M. Ali Ahmad, B. Prelot, A. Razafitianamaharavo, J. M. Douillard, J. Zajac, F. Dufour, O. Durupthy, C. Chaneac and F. d. r. Villiéras, *J. Phys. Chem. C*, 2012, **116**, 24596-24606.

10 M. Ali Ahmad, B. Prelot, F. Dufour, O. Durupthy, A. Razafitianamaharavo, J. M. Douillard, C. Chaneac, F. Villiéras and J. Zajac, *J. Phys. Chem. C*, 2013, **117**, 4459-4469.
11 H. Metiu, S. Chrétien, Z. Hu, B. Li and X. Sun, *J. Phys. Chem. C*, 2012, **116**, 10439-10450.
12 M. Kitano, E. Wada, K. Nakajima, S. Hayashi, S. Miyazaki, H. Kobayashi and M. Hara, *Chem. Mater.*, 2013, **25**, 385-393.
13 J. Pan, G. Liu, G. Q. M. Lu and H. M. Cheng, *Angew. Chem. Int. Ed.*, 2011, **50**, 2133-2137.
14 N. Q. Wu, J. Wang, D. Tafen, H. Wang, J. G. Zheng, J. P. Lewis, X. G. Liu, S. S. Leonard and A. Manivannan, *J. Am. Chem. Soc.*, 2010, **132**, 6679-6685.
15 G. Liu, H. G. Yang, J. Pan, Y. Q. Yang, G. Q. Lu and H.M. Cheng, *Chem. Rev.*, 2014, **114**, 9559-9612.
16 H. G. Yang, C. H. Sun, S. Z. Qiao, J. Zou, G. Liu, S. C. Smith, H. M. Cheng and G. Q. Lu, *Nature*, 2008, **453**, 638-641.
17 A. Vittadini, A. Selloni, F. P. Rotzinger and M. Grätzel, *Phys. Rev. Lett.*, 1998, **81**, 2954-2957.
18 M. Lazzeri, A. Vittadini and A. Selloni, *Phys. Rev. B*, 2001, **63**, 155409.
19 Z. Zhao, Z. Li and Z. Zou, *J. Phys. Chem. C*, 2012, **116**, 7430-7441.
20 F. De Angelis, G. Vitillaro, L. Kavan, M. K. Nazeeruddin and M. Grätzel, *J. Phys. Chem. C*, 2012, **116**, 18124-18131.
21 J. Fan, W. Cai and J. Yu, *Chem. Asian J.*, 2011, **6**, 2481-2490.
22 G. Liu, C. Sun, H. G. Yang, S. C. Smith, L. Wang, G. Q. Lu and H.-M. Cheng, *Chem. Commun.*, 2010, **46**, 755-757.
23 T. L. Xu, P. V. Kamat and K. E. O'Shea, *J. Phys. Chem. A*, 2005, **109**, 9070-9075.
24 H. Lee and W. Choi, *Environ. Sci. Technol.*, 2002, **36**, 3872-3878.
25 J. Ryu and W. Choi, *Environ. Sci. Technol.*, 2006, **40**, 7034-7039.
26 M. A. Ferguson, M. R. Hoffmann and J. G. Hering, *Environ. Sci. Technol.*, 2005, **39**, 1880-1886.
27 G. Zhang, M. Sun, Y. Liu, X. F. Lang, L. M. Liu, H. J. Liu, J. H. Qu and J. H. Li, *ACS Appl. Mater. Interfaces*, 2015, **7**, 511-518.
28 T. Luo, J. Cui, S. Hu, Y. Huang and C. Jing, *Environ. Sci. Technol.*, 2010, **44**, 9094-9098.
29 L. Yan, Y. Huang, J. Cui and C. Jing, *Water Res.*, 2015, **68**, 572-579.
30 J. Cui, J. Shi, G. Jiang and C. Jing, *Environ. Sci. Technol.*, 2013, **47**, 5419-5424.
31 K.-i. Ishibashi, A. Fujishima, T. Watanabe and K. Hashimoto, *J. Photochem. Photobiol., A*, 2000, **134**, 139-142.
32 S. J. Clark, M. D. Segall, C. J. Pickard, P. J. Hasnip, M. I. J. Probert, K. Refson and M. C. Payne, *Z. Kristallogr.*, 2005, **220**, 567-570.
33 L. Yan, S. Hu, J. Duan and C. Jing, *J. Phys. Chem. A*, 2014, **118**, 4759-4765.
34 J. P. Perdew, K. Burke and M. Ernzerhof, *Phys. Rev. Lett.*, 1996, **77**, 3865.
35 S. M. Kemdeo, V. S. Sapkal and G. N. Chaudhari, *J. Mol. Catal. A: Chem.*, 2010, **323**, 70-77.
36 G. He, G. Pan and M. Zhang, *J. Colloid Interface Sci.*, 2011, **364**, 476-481.
37 G. He, G. Pan, M. Zhang and Z. Wu, *J. Phys. Chem. C*, 2009, **113**, 17076-17081.
38 X. Q. Gong and A. Selloni, *J. Phys. Chem. B*, 2005, **109**, 19560-19562.
39 M. Bissen, M. M. Vieillard-Baron, A. J. Schindelin and F. H. Frimmel, *Chemosphere*, 2001, **44**, 751-757.
40 D. Monllor-Satoca, R. Gomez and W. Choi, *Environ. Sci. Technol.*, 2012, **46**, 5519-5527.
41 J. Ryu and W. Choi, *Environ. Sci. Technol.*, 2004, **38**, 2928-2933.
42 C. Richard, *J. Photochem. Photobiol., A*, 1993, **72**, 179-182.
43 C. Richard, F. Bosquet and J. F. Pilichowski, *J. Photochem. Photobiol., A*, 1997, **108**, 45-49.
44 L. F. Lin, S. Althabaiti and R. R. Kuntz, *J. Photochem. Photobiol., A*, 1992, **64**, 93-101.
45 J. Sun, H. Zhang, L.-H. Guo and L. Zhao, *ACS Appl. Mater. Interfaces*, 2013, **5**, 13035-13041.
46 X. Ma, Y. Dai, M. Guo and B. Huang, *Langmuir*, 2013, **29**, 13647-13654.
47 X. Ma, Y. Dai, M. Guo and B. Huang, *J. Phys. Chem. C*, 2013, **117**, 24496-24502.
48 U. Diebold, *Surf. Sci. Rep.*, 2003, **48**, 53-229.
49 J. B. Simonsen, B. Handke, Z. Li and P. J. Møller, *Surf. Sci.*, 2009, **603**, 1270-1275.
50 S. Liu, J. Yu and M. Jaroniec, *Chem. Mater.*, 2011, **23**, 4085-4093.
51 A. Selloni, *Nat Mater*, 2008, **7**, 613-615.
52 G. Liu, H. G. Yang, X. Wang, L. Cheng, H. Lu, L. Wang, G. Q. Lu and H.M. Cheng, *J. Phys. Chem. C*, 2009, **113**, 21784-21788.
53 T. Tachikawa, S. Yamashita and T. Majima, *J. Am. Chem. Soc.*, 2011, **133**, 7197-7204.
54 M. D'Arienzo, J. Carbajo, A. Bahamonde, M. Crippa, S. Polizzi, R. Scotti, L. Wahba and F. Morazzoni, *J. Am. Chem. Soc.*, 2011, **133**, 17652-17661.

Graphical Abstract:

$TiO_2$ {001} facet with strong Lewis acid sites exhibit high adsorption affinity to $O_2$ to generate $O_2^{\bullet-}$ and then oxidize adsorbed As(III).